



# Effect of Velocity and Contact Stress Area on the Dynamic Behavior of the Spinal Cord Under Different Testing Conditions

Chen Jin<sup>†</sup>, Rui Zhu<sup>†</sup>, Meng-lei Xu, Liang-dong Zheng, Hui-zi Zeng, Ning Xie\* and Li-ming Cheng\*

Key Laboratory of Spine and Spinal Cord Injury Repair and Regeneration of Ministry of Education, Orthopaedic Department of Tongji Hospital, Tongji University School of Medicine, Shanghai, China

## OPEN ACCESS

### Edited by:

Ron Noah Alkalay,  
Harvard Medical School,  
United States

### Reviewed by:

Zin Zin Khaing,  
University of Washington,  
United States  
Yuan Feng,  
Shanghai Jiao Tong University, China

### \*Correspondence:

Ning Xie  
nxieprof18@tongji.edu.cn  
Li-ming Cheng  
limingcheng@tongji.edu.cn

<sup>†</sup>These authors have contributed  
equally to this work

### Specialty section:

This article was submitted to  
Biomechanics,  
a section of the journal  
Frontiers in Bioengineering and  
Biotechnology

**Received:** 03 November 2021

**Accepted:** 31 January 2022

**Published:** 04 March 2022

### Citation:

Jin C, Zhu R, Xu M-l, Zheng L-d,  
Zeng H-z, Xie N and Cheng L-m (2022)  
Effect of Velocity and Contact Stress  
Area on the Dynamic Behavior of the  
Spinal Cord Under Different  
Testing Conditions.  
Front. Bioeng. Biotechnol. 10:762555.  
doi: 10.3389/fbioe.2022.762555

Knowledge of the dynamic behavior of the spinal cord under different testing conditions is critical for our understanding of biomechanical mechanisms of spinal cord injury. Although velocity and contact stress area are known to affect external mechanical stress or energy upon sudden traumatic injury, quantitative investigation of the two clinically relevant biomechanical variables is limited. Here, freshly excised rat spinal-cord-pia-arachnoid constructs were tested through indentation using indenters of different sizes (radii: 0.25, 0.50, and 1.00 mm) at various loading rates ranging from 0.04 to 0.20 mm/s. This analysis found that the *ex vivo* specimen displayed significant nonlinear viscoelasticity at <10% of specimen thickness depth magnitudes. At higher velocity and larger contact stress area, the cord withstood a higher peak load and exhibited more sensitive mechanical relaxation responses (i.e., increasing amplitude and speed of the drop in peak load). Additionally, the cord became stiffer (i.e., increasing elastic modulus) and softer (i.e., decreasing elastic modulus) at a higher velocity and larger contact stress area, respectively. These findings will improve our understanding of the real-time complex biomechanics involved in traumatic spinal cord injury.

**Keywords:** spinal cord, velocity, contact stress area, indentation, mechanical response, biomechanics

## INTRODUCTION

Traumatic spinal cord injury (SCI) is a significant health challenge worldwide. SCI disrupts the central nervous system, often causing permanent motor and sensory deficits. Globally, almost 180,000 SCI cases are recorded annually (Devivo, 2012; Noonan et al., 2012; Fitzharris et al., 2014), leading to extensive research into the causes, prevention, and treatment of SCIs.

Due to complicated loading environments during SCI, it is difficult to accurately measure local tissue mechanical forces using animal models. In contrast, computational modeling offers an economical, efficient, and ethical method for investigating the mechanical etiology of SCI, as well as SCI prevention and treatment. Because tissue deformation and stress correlate with injury severity and neurological impairment (Scifert et al., 2002; Maikos et al., 2008a; Li and Dai, 2009; Russell et al., 2012; Khuyagbaatar et al., 2016), finite element computational modeling allows researchers to conduct controlled SCI simulations and predict internal tissue responses and associated injury severity under various conditions (Maikos et al., 2008a; Li and Dai, 2009; Russell et al., 2012). However, to accurately model the spinal cord, accurate and detailed

anatomical geometry and experimental data of cord tissue are needed to correctly predict the stresses and strains produced in the spinal cord during injury. Over the past decades, numerous spinal cord models have been developed (Scifert et al., 2002; Greaves et al., 2008; Li and Dai, 2009; Khuyagbaatar et al., 2016). However, accurate experimental data to characterize the dynamic behavior of spinal cord tissue are still necessary.

Various testing methods, including tensile, compression, and shear, have been used to investigate the mechanical properties of the spinal cord (Shetye et al., 2014; Bartlett et al., 2016; Karimi et al., 2017; Jannesar et al., 2018; Yu et al., 2020). Traumatic SCI is caused by a mechanical force acting upon the spinal cord, leading to linear and rotational accelerations that occur in a mix of compression, tension, and shear. Because indentation causes tension, compression, and shear deformation fields (Lin et al., 2009), it is an ideal loading modality for obtaining material properties of spinal cord tissue for the study of the biomechanics of traumatic SCI. Currently, animal models, including rats, are widely used to study SCI (Li et al., 2018). However, to our knowledge, few studies have investigated the microscale mechanical properties of rat spinal cord tissue through indentation. Here, we used the indentation test method to characterize the mechanical response of the spinal cord under different testing conditions and to understand the effects of velocity and contact stress area on the spinal cord.

## MATERIALS AND METHODS

### Specimen Preparation

Animal experiment protocols were approved by the animal welfare committee at Tongji Hospital affiliated with Tongji University, Shanghai. To avoid potential sex effects, the analyses used female adult Sprague-Dawley rats (260–280 g), aged >10 weeks, at which they are considered to have mature spinal cords (Clarke et al., 2009). To collect accurate constitutive data from mechanical experiments, normal spinal cord tissue specimens were collected in a way that limited damage to the organ. To this end, rats were killed by intraperitoneal injection of a lethal dose of pentobarbitone sodium (100 mg/kg) and permanent cessation of circulation confirmed by cardiac perfusion with ice-cold phosphate-buffered saline (PBS; pH 7.4). A dorsal laminectomy was then performed, and nerve roots were carefully severed. The spinal cord was then cut at the seventh cervical vertebra and the first lumbar vertebra, and harvested thoracic spinal cord segments were immediately soaked in PBS (4°C). The dura mater was carefully removed. Damaged cords were excluded from the study. Notably, we referred to this specimen as “spinal cord and pia-arachnoid complex (SCPC)” (Ramo et al., 2018a; Ramo et al., 2018b). Next, the specimens were oriented with the ventral surface facing up, attached on a slide using cyanoacrylate adhesive, and placed in a 100-mm-diameter culture dish and covered with PBS to prevent dehydration. The culture dish was then positioned under the indenter tip and the specimen equilibrated for 10 min before indentation testing. To limit proteolysis and necrosis,

indentation tests were done at room temperature (24°C) within an hour of the death of the rats, as post-mortem time can greatly affect the mechanical properties of biological tissues (Bilston and Thibault, 1995).

### Indentation Setup

A schematic of the setup of indentation load–relaxation tests on SCPC tissues is shown in **Figure 1**. Mechanical properties were measured *ex vivo* using a Mach-1 Model V500css device (Biomomentum Inc., Laval, QC, Canada). The technique precisely assessed surface orientation at each position and recorded normal load with a single-axial load cell (1.5 N range and 0.07 mN resolution on the vertical axis). The Mach-1 micromechanical system was made of the tester frame, three motorized stages, one motion controller, one load cell, one load cell amplifier, one computer, and accessories such as testing chambers and fixtures. The load cell amplifier powered the load cell and converted the measured force signal into a digital value that was relayed to a computer. The stage was commanded using a motion controller, which was in turn controlled by the Mach-1 Motion software.

### Indentation Protocol

To systematically characterize the mechanical response of the SCPC tissue, indenter size, indentation displacement, and loading velocity were introduced as experimental parameters. With regards to indenter size, spherical indenters with radii of 0.25, 0.50, and 1.00 mm were used in this study. For loading velocity, loads of 0.04, 0.06, 0.08, 0.10, 0.15, and 0.20 mm/s were applied to each indenter. The indentation protocol consisted of a single indent with an indentation amplitude of 0.25 mm (i.e., 8.3% of the specimen thickness), which lay within the recommended range of 10% to minimize boundary effects (Garo et al., 2007). The relaxation time was set to 30 s. Data with a displacement error of >5% were discarded. Data were collected at a 100-Hz sampling frequency.

Indentation locations were chosen at random for each specimen. Test order was randomized for each specimen to minimize order effects. The indentation system was operated in displacement control mode during loading. Specimens did not undergo any other preconditioning before experiments. Indentation was done at a velocity of 0.04–0.20 mm/s at six different random sites for each specimen. Between tests, the specimen was allowed to recover for 100 s. Because of the high dissipative nature of neural tissues (Shulyakov et al., 2011), specimens were discarded after indentation. Repetitive tests were performed on 10 different rats.

### Data Analysis

Indentation load–relaxation curves consisted of an indentation and a relaxation portion (**Figure 2**). In the indentation portion, indenters were indented into the tissue at different constant velocities and held during the relaxation portion. Mean peak loads at maximum indentation depth and mean loads at 5, 10, 15, 20, 25, and 30 s during the relaxation phase were calculated to characterize temporal variations.

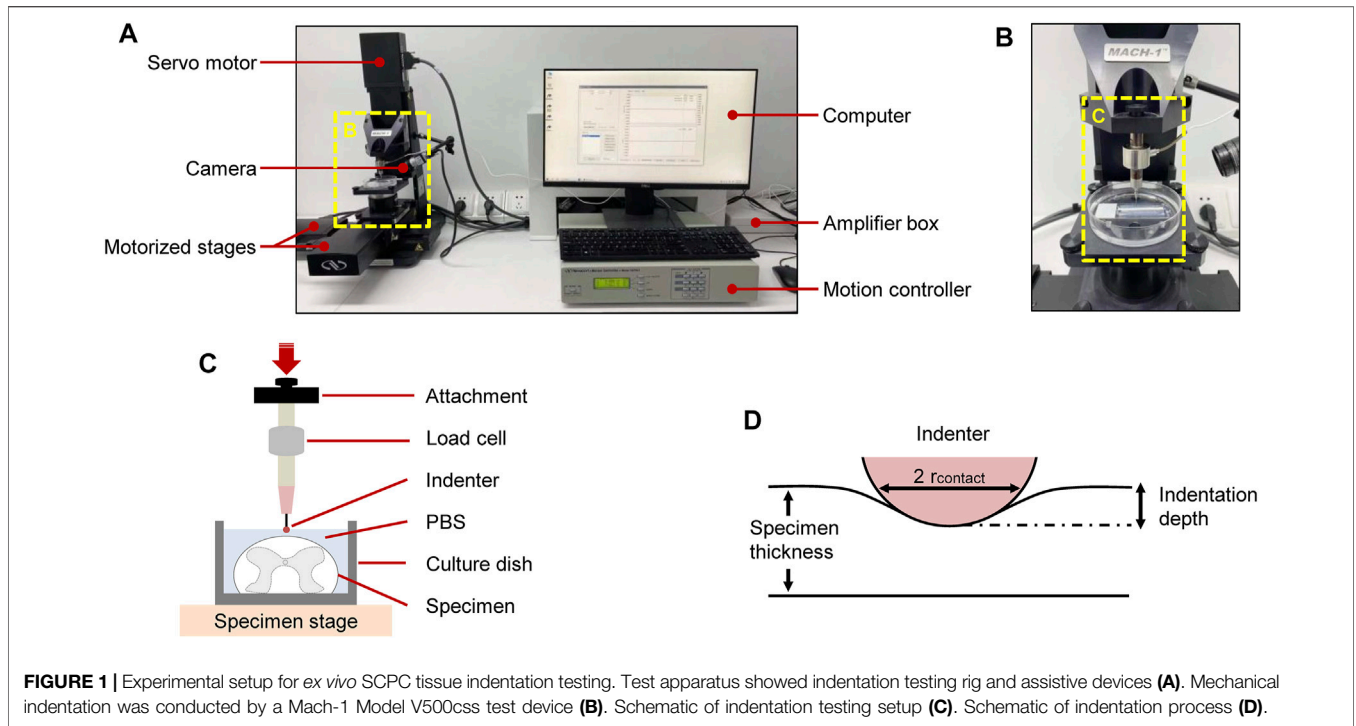


**FIGURE 1** | Experimental setup for *ex vivo* SCPC tissue indentation testing. Test apparatus showed indentation testing rig and assistive devices (A). Mechanical indentation was conducted by a Mach-1 Model V500css test device (B). Schematic of indentation testing setup (C). Schematic of indentation process (D).

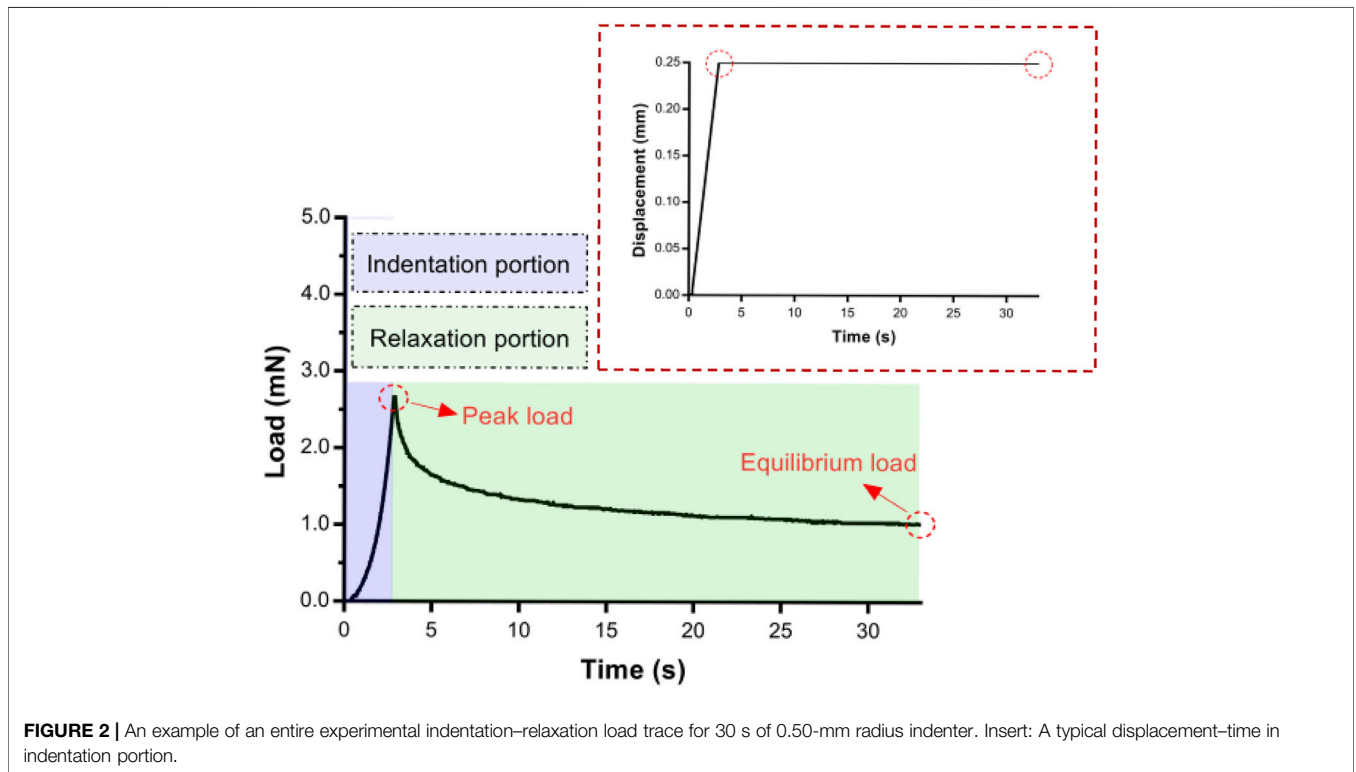
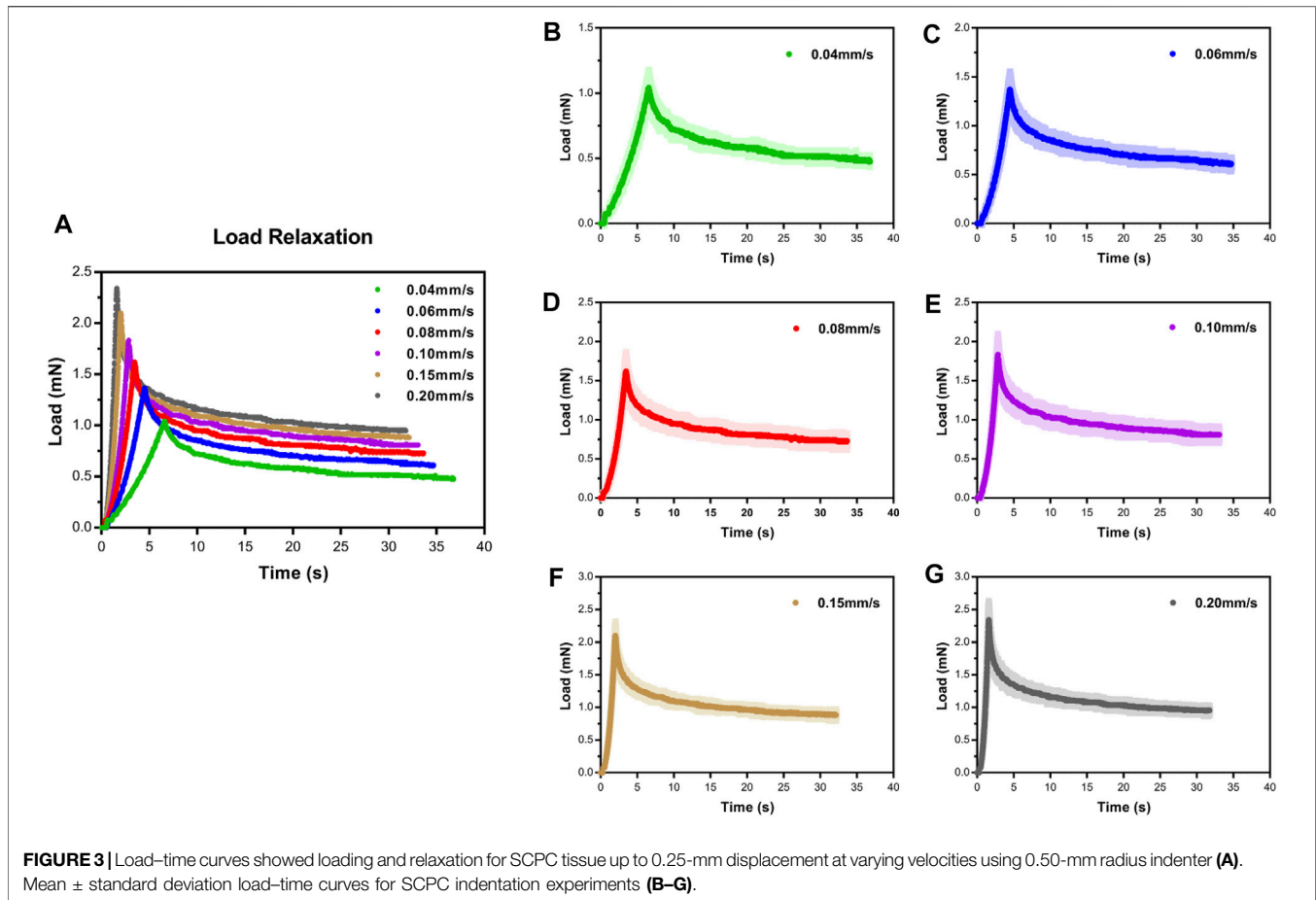


**FIGURE 2** | An example of an entire experimental indentation–relaxation load trace for 30 s of 0.50-mm radius indenter. Insert: A typical displacement–time in indentation portion.

The elastic modulus (EM) was determined in the form of an indentation method using a spherical indenter. Areas of interest were identified across the surface of each specimen by visual inspection. Indentation load–displacement curves were

performed on each region using a Mach-1 Model V500css test device. Indentation parameters were kept constant for each specimen (displacement: 0.25 mm, relaxation time: 30 s). EM at each position was determined by fitting the load–displacement



curve with corresponding thickness and an effective Poisson's ratio of 0.5 (Saxena et al., 2012) to an elastic model for indentation as described before (Hayes et al., 1972) (see Eq. 1) using the Mach-1 analysis software (version 6.3, Biomomentum Inc., Laval, QC, Canada). This model is well suited for the mechanical description of specimens bound to flat rigid support (at least 10 times stiffer than the specimen).

$$EM = \frac{P}{H} \times \frac{1 - \nu^2}{2ak\left(\frac{a}{h}, \nu\right)} \quad (1)$$

where  $P$  = load,  $H$  = indentation displacement,  $\nu$  = Poisson's ratio,  $a$  = radius of the contact region,  $k$  = correction factor dependent on  $a/h$  and  $\nu$ , and  $h$  = specimen thickness.

## Statistical Analysis

Statistical analyses and graphical representation were done on SPSS version 20.0 (SPSS, Inc., Chicago, IL, USA) or GraphPad Prism version 7.0 (GraphPad Software Inc., San Diego, CA, USA). Differences between the two groups were compared using a two-tailed Student's  $t$ -test. Non-normally distributed data were compared using the Mann–Whitney–Wilcoxon test. Multiple group comparisons used one-way analysis of variance with Tukey's *post-hoc* test where there was homogeneity of variances or Tamhane *post-hoc* test where variances were

unequal. Exact  $p$ -values are reported in **Supplementary Tables S1**.  $p \leq 0.05$  indicated statistically significant differences.

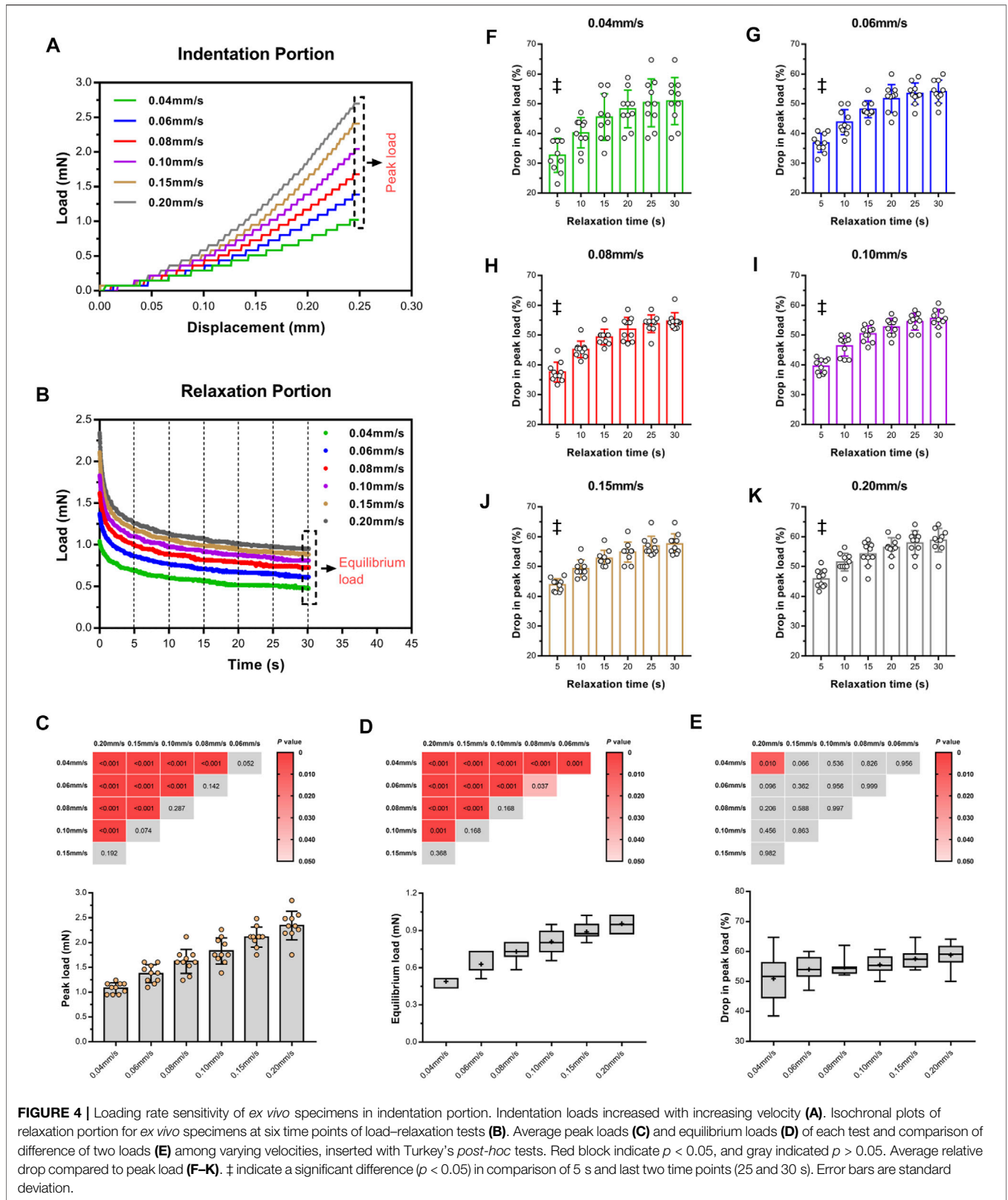
## RESULTS

### General Mechanical Response

From the contact point onward, the load recording was stable (Figure 2). The indentation depth was held at a maximum of 0.25 mm (up to peak load), and the load decreased upon relaxation.

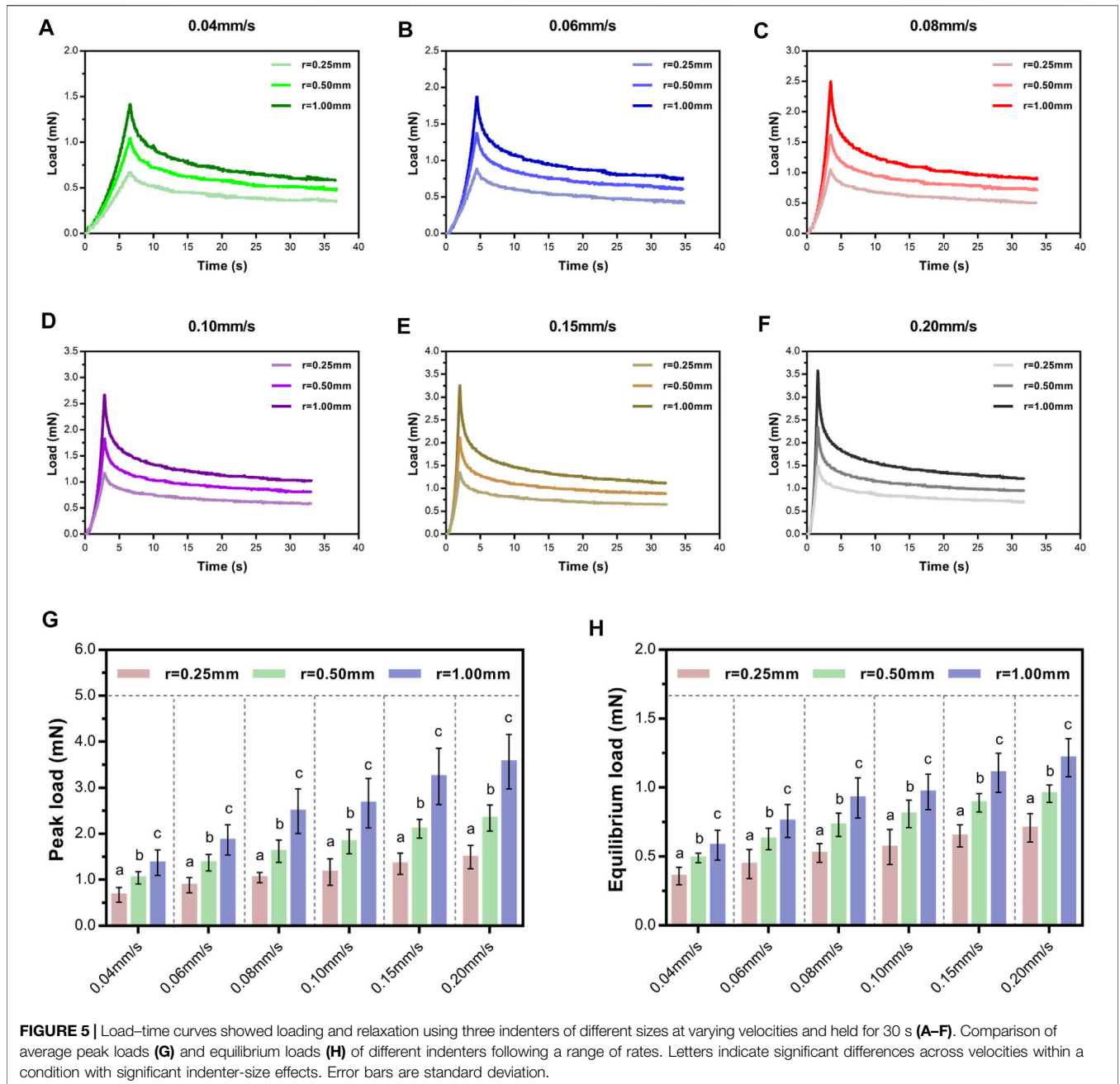
### Effect of Velocity

To assess the influence of velocity on the cord, we performed a series of single indents at velocities of 0.04–0.20 mm/s. We then analyzed the viscoelastic behavior of the specimen during the indentation load–relaxation period and recorded average load curves at different rates for the 0.50-mm indenter (Figure 3). The mechanical behavior observed during this study was typical of biological materials, with the initial ramp region showing a nonlinear increase in load with applied displacement (taking the form of a “J”), with the load at first being compliant and rising slowly before gradually steepening until maximum applied indentation depth was reached (Figure 4A). Moreover, the ramping slope of higher rates was greater than that of lower rates. As expected for viscoelastic materials, in all conditions,



peak load increased with increasing velocity. Relaxation portion data at various loading rates are shown in Figure 4B. The curve showed that most peak load decay occurred in the initial phase

(0–5 s). After approximately 10 s, the load converged gradually toward its static equilibrium value. The degree of load relaxation present was approximately 50–60% of the initial peak load over

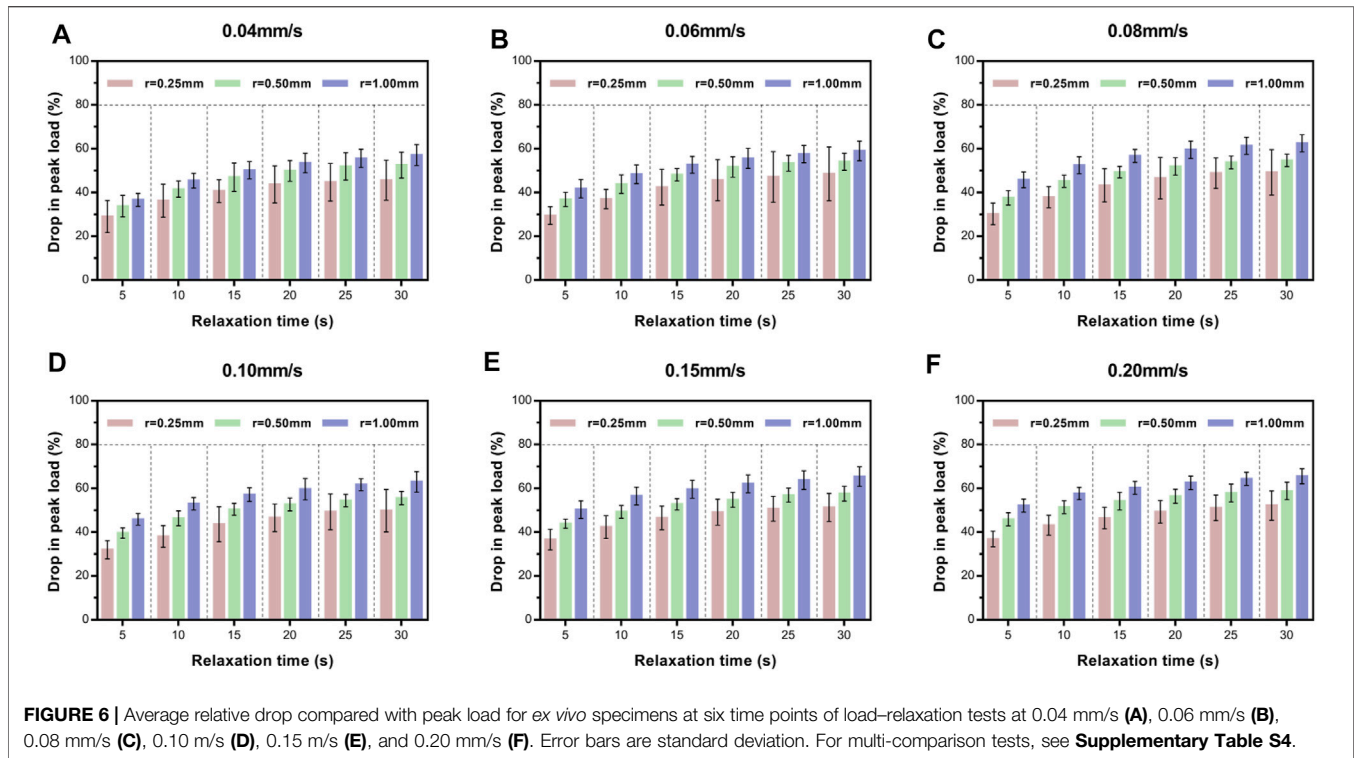


the 30-s period. The peak loads obtained at rates of 0.04–0.20 mm/s were  $1.08 \pm 0.11$ ,  $1.37 \pm 0.18$ ,  $1.62 \pm 0.24$ ,  $1.83 \pm 0.26$ ,  $2.11 \pm 0.20$ ,  $2.34 \pm 0.29$  mN, respectively (Figure 4C). Notably, long-term (equilibrium) load after relaxation varied with the loading rate, with higher-rate tests exhibiting larger equilibrium loads at the end of the relaxation period (Figure 4D). Analysis of decay (percentage) between peak and equilibrium load revealed no significant differences at different velocities (Figure 4E).

Figures 4F–K quantitatively display the average drop values in peak load of the specimens at six equidistant time points at various loading rates. At the first isochrone (5 s) examined tests,

the specimens showed a significant decay than the last two time points (25 and 30 s) ( $p < 0.001$ , Supplementary Table S1). In comparison with lower rates, higher rates exhibited a larger drop in peak load for the SCPC tissues at the same isochrones, indicating that the tissues responded more quickly.

Next, we repeated the indentation load–relaxation tests with 0.25- and 1.00-mm indenters at each rate (Supplementary Figures S1,2; Supplementary Tables S2,3). Similar response trends were observed across all indentation tests. To demonstrate the usefulness and applicability of the current data, we further repeated the indentation experiments on the larger animal models (i.e., mature ewes) (N = 6). The results



between these two species were similar, suggesting the strong velocity-dependent nature of the SCPC tissue (**Supplementary Figure S3**).

### Effect of Contact Stress Area

Here, the variance of contact stress area from common compression factors such as fracture fragment, herniated intervertebral disc, and osteophyte was made by altering the spherical tip radius. Representative indentation and relaxation behaviors of SCPC tissues using spherical indenters with radii of 0.25, 0.5, and 1.00 mm at rates of 0.04–0.20 mm/s are shown in **Figures 5A–F**. Comparison of peak and equilibrium loads among the three indenters at each rate revealed that load depended on indenter size and significantly increased in magnitude with increasing indenter radius at a constant velocity ( $p \leq 0.01$ , Tukey–Kramer multi-comparison test, **Figures 5G, H**).

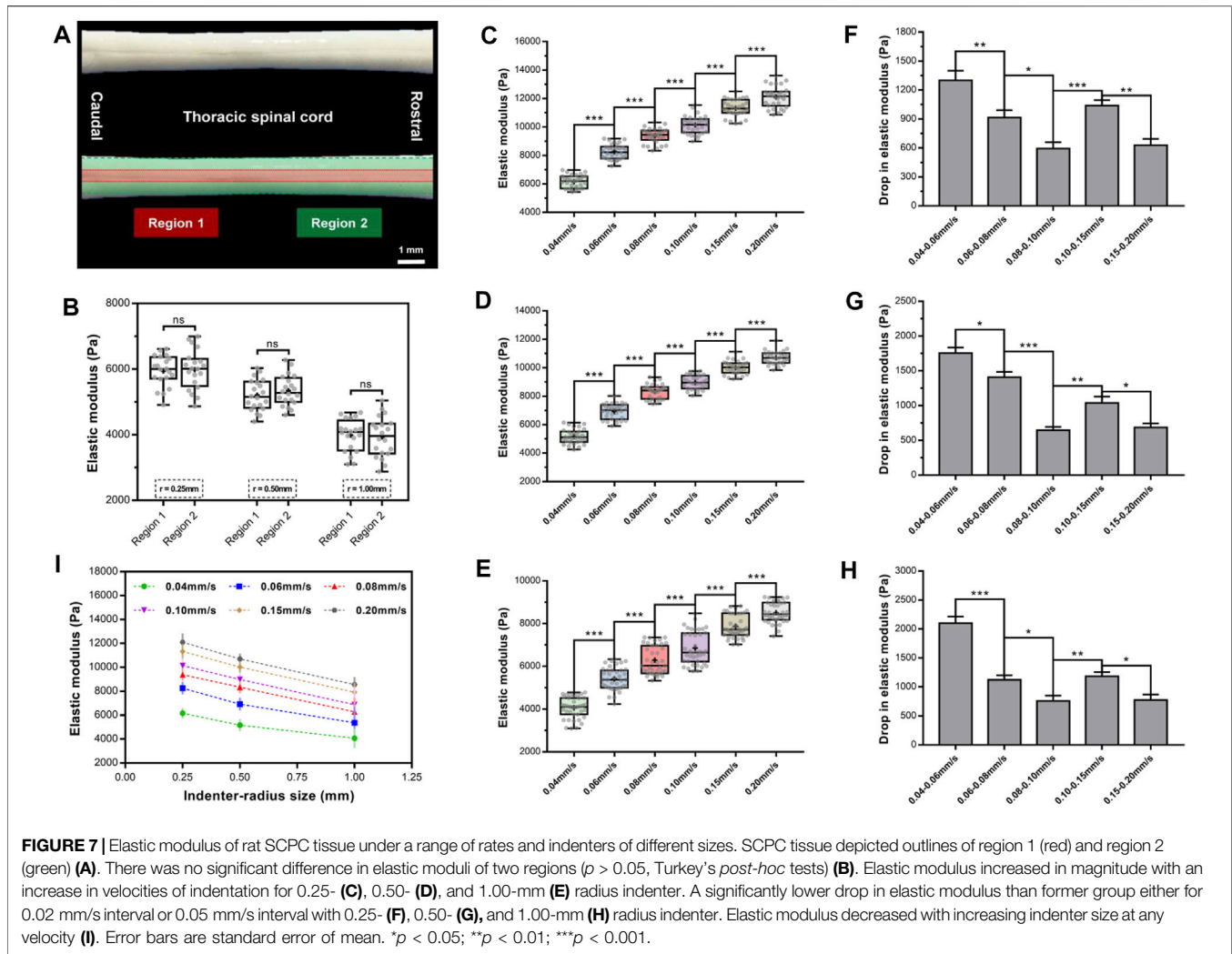
Next, we investigated the effect of indenter size on peak load decay in the relaxation portion (**Figure 6**). For a given velocity (e.g., 0.04 mm/s), larger contact areas exhibited larger drops in peak load at the same isochrones. Turkey's *post-hoc* tests or Tamhane *post-hoc* tests within each indenter to test the statistical significance of the drop in peak load at different relaxation time points (**Supplementary Table S4**) revealed that the contact stress area indeed significantly influenced the drop in peak load.

### Elastic Modulus of the Rat Spinal Cord And Pia-Arachnoid Complex

We first evaluated the mechanical characteristics and spatial heterogeneity of the elastic properties of rat SCPC tissues

(**Figure 7A**). We defined two tissue regions (Devivo, 2012; Noonan et al., 2012), corresponding to the intermediate zone and marginal zone based on the visual appearance of the ventral surface of the specimen. Inevitably, some diversities were observed for the repetitive experiments due to structural heterogeneity. These differences were not statistically significant (**Figure 7B**). This indicates that normal SCPC tissue stiffness was spatially relatively homogeneous with low variation in elastic values, which is consistent with past findings (Cooper et al., 2020). The stiffness of regions one and two did not differ significantly across specimens ( $p \geq 0.05$ , **Supplementary Figure S4, Supplementary Table S5**).

To investigate the effect of velocity on EM, we assessed changes in tissue elasticity at 0.04, 0.06, 0.08, 0.10, 0.15, and 0.20 mm/s at an indentation depth of 0.25 mm and averaged mean EM values from 10 force curves, per area. This analysis found that for all three indenters, the EM of the SCPC tissue was significantly depended on indentation velocity and increased in magnitude with increasing indentation velocity (**Figures 7C–E, Supplementary Table S6**). For the 0.25-mm indenter, at indentation velocities of 0.04–0.20 mm/s, the average EM of SCPC tissue increased from 6,163 to 12,103 Pa, for the 0.50-mm indenter, average EM increased from 5,171 to 10,703 Pa, and for the 1-mm indenter, average EM increased from 4,074 to 8,520 Pa. No inter-animal variability was observed for the EM calculated at each rate ( $p \geq 0.05$ , **Supplementary Figure S5, Supplementary Table S7**). For all three indenters, similar elastic behavior was observed with increasing indentation velocity, which is consistent with previous observations (Budday et al., 2015).



Statistical comparisons were performed of EM within the same interval (0.02 or 0.05 mm/s). The 0.08–0.10 mm/s group exhibited a significantly lower drop in elastic stiffness than the 0.06–0.08 mm/s group, and the 0.08–0.10 mm/s group exhibited a significantly lower drop in elastic stiffness than the 0.04–0.06 mm/s group ( $p \leq 0.05$ , **Figures 7F–H, Supplementary Table S8**). Similarly, the 0.15–0.20 mm/s group exhibited a significantly lower drop in elastic stiffness than the 0.10–0.15 mm/s group ( $p \leq 0.05$ , **Figures 7F–H, Supplementary Table S8**).

**Figure 7I** shows the effect of indenter size on EM. This analysis found that EM decreased with increasing indenter size. For example, at the rate of 0.04 mm/s and indenter radii of 0.25–1.00 mm, the average EM decreased from 6,163 to 4,074 Pa.

## DISCUSSION

Here, we characterized the mechanical properties of post-mortem rat SCPC tissue *ex vivo*, using indentation testing and

quantitatively described mechanical response of the compressed tissue under various loading rates and indenter sizes.

Comparisons between different velocities revealed a strong velocity-dependent nature of SCPC tissue. The indentation tests showed a greater peak load (i.e., stress) upon the spinal cord with the higher initial speed in the ramp or relaxation phase. These results indicate a velocity threshold: speed of impact above that threshold will cause additional damage, whereas speed of impact below that threshold will not be damaging. Increasing speed leading to further injure the cord was consistent with our understanding of tissue mechanics, as more energy could be transferred to the spinal cord, causing damage (Lam et al., 2014). Past studies indicated that damage to neurons and astrocytes occurred at strain rates between 10 and 30/s (Cullen et al., 2007), whereas damage to microtubules occurred at 44/s (Ahmadzadeh et al., 2014).

Interestingly, significant relaxation was observed at all loading rates, with the largest degree of relaxation (i.e., drop in peak load) occurring at the initial 5 s in the relaxation portion. In previous studies, load relaxation behavior has been shown to depend on initial speed, where stress on the cord tissue relaxed more rapidly



after a high-rate injury when compared with a slow rate (Carlson et al., 1997a; Carlson et al., 1997b). It is reported that due to the high-velocity nature of the injury, force decreased dramatically to <50% of the peak force within 5–10 s of initial impact (Sjovold et al., 2013), which is consistent with our findings. We inferred that the contribution of this positive mechanical response of the cord might distribute the total load, avoiding local stress concentration. From a clinical standpoint, this suggested that the dynamic behavior of SCPC tissue under high-energy pathological conditions is more sensitive than in low-energy pathological conditions.

Few researchers have investigated the impact of contact stress area on the SCPC tissue. A recent meta-analysis examined several clinically biomechanical factors related to SCI in preclinical studies, attempting to accurately determine effect sizes for each (Batchelor et al., 2013). In that meta-analysis, one of the most important factors identified is compressive pressure, with a power-law distribution being observed between compressive pressure and time to severe neurological injury. In our study, the larger indenter resulted in greater load at the same indentation depth relative to the smaller indenter, indicating that the spinal cord might suffer from a greater degree of external mechanical force and high risk of damage in a similar clinical setting. However, the EM of the SCPC tissue decreased monotonically with increasing tip size, which is consistent with previous findings (Simha et al., 2007). A possible reason for this was its inhomogeneous structure. Assessments at time (~s) and length scales (~mm) relevant to cell physiology found that central nervous system tissue was mechanically heterogeneous (Elkin et al., 2007; Christ et al., 2010; Elkin et al., 2011; Iwashita et al., 2014). A recent paper also indicated that stiffness distributions under compression strongly correlated with axon orientation, areas of cell nuclei, and cellular in plane proximity (Koser et al., 2015). Unfortunately, there is no way of avoiding such potential causes from the indentation test data alone. However, the use of multiple indenters may give valuable information on the organization and integrity of the cord, providing a way to relate SCPC properties to tissue microstructure.

Because SCPC tissue is viscoelastic, its modulus (or stiffness) varies under various experimental parameters. However, the influence factors of calculating EM were taken little attention (Bilston and Thibault, 1995; Bilston et al., 2001; Fiford and Bilston, 2005). Whether or not to precondition is controversial, with some researchers suggesting that preconditioning reduces inter-specimen variability (Fallenstein et al., 1969; Bilston et al., 1997; Cheng et al., 2009), whereas others suggest it may confound and influence end modulus measurements due to changes in cord microstructure and different patterns of fluid redistribution in the spinal cord (Ichihara et al., 2001). Thus, researchers must be aware that preconditioning may change tissue architecture and confound conclusions. Another important consideration is the region and orientation of the tested tissue specimen. Here, we did not identify significant differences in stiffness between different regions of the SCPC tissues. Although numerous studies found that gray matter was stiffer than white matter (Prange and Margulies, 2002; Christ et al., 2010; van Dommelen et al.,

2010; Koser et al., 2015), others found the opposite (Ozawa et al., 2001; Kruse et al., 2008; Budday et al., 2015), whereas others observed no significant differences in the moduli of white and gray matter (Maikos et al., 2008b; Finan et al., 2012). This was a challenging question to answer because of the high complexity of neural tissue with anisotropic and inhomogeneous mechanical properties (Koser et al., 2015; Cooper et al., 2020). Furthermore, different experimental techniques had unique strengths and limitations and operated at divergent length scales (Budday et al., 2015).

The dura mater is the outermost and most substantial meningeal layer of spinal cord tissue that protects the spinal cord. The rat spinal dura has a modulus in tension that is two orders of magnitude greater than the stiffness of rat spinal cord (Fiford and Bilston, 2005). In animal models of traumatic SCI, the external forces and/or mechanical damages are often transmitted to the dura mater to injure the underlying SCPC tissue. So, the dura will contribute significantly to the overall mechanical response of the spinal cord to traumatic loading and may absorb a large percentage of the kinetic energy (Maikos et al., 2008b). As such, some investigators have suggested removing dura mater to accurately determine how the underlying tissue (i.e., SCPC) responds in the compression stage and the mechanical properties of the SCPC tissue (Clarke et al., 2009; Ramo et al., 2018a). Although the spinal cord tissue is normally not injured from protrusions under the dura in a clinical scenario, the severity of neurological impairment primarily correlates with the degree of substantial damage to the spinal cord parenchyma, according to several previous histopathological studies (Chen et al., 2016). Thus, we believe that it is meaningful and important to directly investigate the dynamic behavior of the SCPC. Additionally, the cord is immersed by cerebrospinal fluid (CSF) that acts as a protecting shock absorber, and it is believed that the response of the CSF cannot be ignored when considering the mechanics of the spinal cord (Persson et al., 2011; Arhaptsov and Marom, 2021). Moreover, without removing the dura, it is experimentally difficult to accurately simulate and measure the *in vivo* CSF pressure in *ex vivo* conditions, limiting the capacity to quantitatively identify the mechanical characteristics of the whole spinal cord tissue. Therefore, we mainly focused on the dynamic behavior of the SCPC without considering the complex effects of dura mater and CSF.

This study has some limitations. First, *ex vivo* analyses do not adequately represent *in vivo* conditions. Even when using optimized storage conditions, CSF pressure and tissue degradation may lead to differences in viscoelastic features in *ex vivo* tissue versus *in vivo* cord tissue (Metz et al., 1970; Etz et al., 2009). However, because the protocols used by these studies are not the same as ours, direct comparisons cannot be made. Future studies will investigate this *in vivo*. Another important limitation is the geometry of the indenter. To ensure accuracy in the comparison of the results calculated from various indenters, we did not use conical or plane-ended cylindrical indenters to simulate the contact stress area of different geometries. However, although the elastic model used to fit the experimental data

depended on the geometry of the indenter, the theory of contact mechanics has been well established (McKee et al., 2011). Finally, the 30 s of relaxation might not be enough to identify the long-term relaxation behavior. Future studies will be enhanced by increasing relaxation time to investigate more information on the viscoelastic behavior of the SCPC tissue.

## CONCLUSION

In conclusion, we comprehensively characterized the regional dynamic behavior of rat SCPC tissue and analyzed the biomechanical effect of velocity and contact stress area on the spinal cord using indentation testing. Our data show that the cord exhibits distinct nonlinear viscoelasticity at <10% of specimen thickness depth magnitudes. At higher velocity and larger contact stress area, the cord withstood a higher peak load and exhibited a more sensitive mechanical relaxation response (i.e., increasing amplitude and speed of drop in peak load), especially the initial phase of residual compression. The cord also became stiffer (i.e., increasing EM) with higher velocity and softer (i.e., decreasing EM) with a larger contact stress area. These findings will improve our understanding of the real-time complex biomechanics involved in traumatic SCI.

## DATA AVAILABILITY STATEMENT

The original contributions presented in the study are included in the article/**Supplementary Material**, further inquiries can be directed to the corresponding authors.

## REFERENCES

- Ahmadzadeh, H., Smith, D. H., and Shenoy, V. B. (2014). Viscoelasticity of Tau Proteins Leads to Strain Rate-dependent Breaking of Microtubules during Axonal Stretch Injury: Predictions from a Mathematical Model. *Biophysical J.* 106, 1123–1133. doi:10.1016/j.bpj.2014.01.024
- Arhiptsov, K., and Marom, G. (2021). Numerical Models of Spinal Cord Trauma: The Effect of Cerebrospinal Fluid Pressure and Epidural Fat on the Results. *J. Neurotrauma* 38 (15), 2176–2185. doi:10.1089/neu.2021.0065
- Bartlett, R. D., Choi, D., and Phillips, J. B. (2016). Biomechanical Properties of the Spinal Cord: Implications for Tissue Engineering and Clinical Translation. *Regenerative Med.* 11, 659–673. doi:10.2217/rme-2016-0065
- Batchelor, P. E., Wills, T. E., Skeers, P., Battistuzzo, C. R., Macleod, M. R., Howells, D. W., et al. (2013). Meta-analysis of Pre-clinical Studies of Early Decompression in Acute Spinal Cord Injury: a Battle of Time and Pressure. *PLoS One* 8, e72659. doi:10.1371/journal.pone.0072659
- Bilston, L. E., Liu, Z., and Phan-Thien, N. (2001). Large Strain Behaviour of Brain Tissue in Shear: Some Experimental Data and Differential Constitutive Model. *Biorheology* 38, 335–345.
- Bilston, L. E., Liu, Z., and Phan-Thien, N. (1997). Linear Viscoelastic Properties of Bovine Brain Tissue in Shear. *Bir* 34, 377–385. doi:10.3233/bir-1997-34603
- Bilston, L. E., and Thibault, L. E. (1995). The Mechanical Properties of the Human Cervical Spinal cord In Vitro. *Ann. Biomed. Eng.* 24, 67–74. doi:10.1007/bf02770996
- Budday, S., Nay, R., de Rooij, R., Steinmann, P., Wyrobek, T., Ovaert, T. C., et al. (2015). Mechanical Properties of gray and white Matter Brain Tissue by

## ETHICS STATEMENT

The animal study was reviewed and approved by the Animal Welfare Committees at Tongji Hospital affiliated with Tongji University in Shanghai.

## AUTHOR CONTRIBUTIONS

CJ and RZ: conception and design, acquisition of data, analysis and interpretation of data, and drafting the article. CJ and RZ contributed equally to this work. M-X, L-Z, and H-Z: analysis and interpretation of data and editing the article. NX and L-C: conception and design, study supervision, and revising the article. All authors contributed to the article and approved the submitted version.

## FUNDING

This work was supported by the National Key R and D Program of China (grant no. 2020YFC2008703), the Science and Technology Commission of Shanghai Municipality (grant no.19411962900) and the National Natural Science Foundation of China (grant no. 81974190).

## SUPPLEMENTARY MATERIAL

The Supplementary Material for this article can be found online at: <https://www.frontiersin.org/articles/10.3389/fbioe.2022.762555/full#supplementary-material>

- Indentation. *J. Mech. Behav. Biomed. Mater.* 46, 318–330. doi:10.1016/j.jmbbm.2015.02.024
- Carlson, G. D., Minato, Y., Okada, A., Gorden, C. D., Warden, K. E., Barbeau, J. M., et al. (1997a). Early Time-dependent Decompression for Spinal Cord Injury: Vascular Mechanisms of Recovery. *J. Neurotrauma* 14, 951–962. doi:10.1089/neu.1997.14.951
- Carlson, G. D., Warden, K. E., Barbeau, J. M., Bahniuk, E., Kutina-Nelson, K. L., Biro, C. L., et al. (1997b). Viscoelastic Relaxation and Regional Blood Flow Response to Spinal Cord Compression and Decompression. *Spine* 22, 1285–1291. doi:10.1097/00007632-199706150-00002
- Chen, K., Liu, J., Assinck, P., Bhatnagar, T., Streijger, F., Zhu, Q., et al. (2016). Differential Histopathological and Behavioral Outcomes Eight Weeks after Rat Spinal Cord Injury by Contusion, Dislocation, and Distraction Mechanisms. *J. Neurotrauma* 33 (18), 1667–1684. doi:10.1089/neu.2015.4218
- Cheng, S., Clarke, E. C., and Bilston, L. E. (2009). The Effects of Preconditioning Strain on Measured Tissue Properties. *J. Biomech.* 42, 1360–1362. doi:10.1016/j.jbiomech.2009.03.023
- Christ, A. F., Franze, K., Gautier, H., Moshayedi, P., Fawcett, J., Franklin, R. J. M., et al. (2010). Mechanical Difference between white and gray Matter in the Rat Cerebellum Measured by Scanning Force Microscopy. *J. Biomech.* 43, 2986–2992. doi:10.1016/j.jbiomech.2010.07.002
- Clarke, E. C., Cheng, S., and Bilston, L. E. (2009). The Mechanical Properties of Neonatal Rat Spinal Cord *In Vitro*, and Comparisons with Adult. *J. Biomech.* 42, 1397–1402. doi:10.1016/j.jbiomech.2009.04.008
- Cooper, J. G., Sicard, D., Sharma, S., Van Gulden, S., McGuire, T. L., Cajiao, M. P., et al. (2020). Spinal Cord Injury Results in Chronic Mechanical Stiffening. *J. Neurotrauma* 37, 494–506. doi:10.1089/neu.2019.6540

- Cullen, D. K., Simon, C. M., and LaPlaca, M. C. (2007). Strain Rate-dependent Induction of Reactive Astrogliosis and Cell Death in Three-Dimensional Neuronal-Astrocytic Co-cultures. *Brain Res.* 1158, 103–115. doi:10.1016/j.brainres.2007.04.070
- Devivo, M. J. (2012). Epidemiology of Traumatic Spinal Cord Injury: Trends and Future Implications. *Spinal Cord* 50, 365–372. doi:10.1038/sc.2011.178
- Elkin, B. S., Azeloglu, E. U., Costa, K. D., and Morrison III, B., 3rd (2007). Mechanical Heterogeneity of the Rat Hippocampus Measured by Atomic Force Microscope Indentation. *J. Neurotrauma* 24, 812–822. doi:10.1089/neu.2006.0169
- Elkin, B. S., Iankovan, A. I., and Morrison, B., 3rd (2011). A Detailed Viscoelastic Characterization of the P17 and Adult Rat Brain. *J. Neurotrauma* 28, 2235–2244. doi:10.1089/neu.2010.1604
- Etz, C. D., Di Luozzo, G., Zoli, S., Lazala, R., Plestis, K. A., Bodian, C. A., et al. (2009). Direct Spinal Cord Perfusion Pressure Monitoring in Extensive Distal Aortic Aneurysm Repair. *Ann. Thorac. Surg.* 87, 1764–1774. doi:10.1016/j.athoracsurg.2009.02.101
- Fallenstein, G. T., Hulce, V. D., and Melvin, J. W. (1969). Dynamic Mechanical Properties of Human Brain Tissue. *J. Biomech.* 2, 217–226. doi:10.1016/0021-9290(69)90079-7
- Fiford, R. J., and Bilston, L. E. (2005). The Mechanical Properties of Rat Spinal Cord *In Vitro*. *J. Biomech.* 38, 1509–1515. doi:10.1016/j.jbiomech.2004.07.009
- Finan, J. D., Elkin, B. S., Pearson, E. M., Kalbian, L. L., and Morrison, B., 3rd (2012). Viscoelastic Properties of the Rat Brain in the Sagittal Plane: Effects of Anatomical Structure and Age. *Ann. Biomed. Eng.* 40, 70–78. doi:10.1007/s10439-011-0394-2
- Fitzharris, M., Cripps, R. A., and Lee, B. B. (2014). Estimating the Global Incidence of Traumatic Spinal Cord Injury. *Spinal Cord* 52, 117–122. doi:10.1038/sc.2013.135
- Garo, A., Hrapko, M., van Dommelen, J. A., and Peters, G. W. (2007). Towards a Reliable Characterisation of the Mechanical Behaviour of Brain Tissue: The Effects of post-mortem Time and Sample Preparation. *Biorheology* 44, 51–58.
- Greaves, C. Y., Gadala, M. S., and Oxland, T. R. (2008). A Three-Dimensional Finite Element Model of the Cervical Spine with Spinal Cord: an Investigation of Three Injury Mechanisms. *Ann. Biomed. Eng.* 36, 396–405. doi:10.1007/s10439-008-9440-0
- Hayes, W. C., Keer, L. M., Herrmann, G., and Mockros, L. F. (1972). A Mathematical Analysis for Indentation Tests of Articular Cartilage. *J. Biomech.* 5, 541–551. doi:10.1016/0021-9290(72)90010-3
- Ichihara, K., Taguchi, T., Shimada, Y., Sakuramoto, I., Kawano, S., and Kawai, S. (2001). Gray Matter of the Bovine Cervical Spinal Cord Is Mechanically More Rigid and Fragile Than the White Matter. *J. Neurotrauma* 18, 361–367. doi:10.1089/08977150151071053
- Iwashita, M., Kataoka, N., Toida, K., and Kosodo, Y. (2014). Systematic Profiling of Spatiotemporal Tissue and Cellular Stiffness in the Developing Brain. *Development* 141, 3793–3798. doi:10.1242/dev.109637
- Jannesar, S., Allen, M., Mills, S., Gibbons, A., Bresnahan, J. C., Salegio, E. A., et al. (2018). Compressive Mechanical Characterization of Non-human Primate Spinal Cord White Matter. *Acta Biomater.* 74, 260–269. doi:10.1016/j.actbio.2018.05.002
- Karimi, A., Shojaei, A., and Tehrani, P. (2017). Mechanical Properties of the Human Spinal Cord under the Compressive Loading. *J. Chem. Neuroanat.* 86, 15–18. doi:10.1016/j.jchemneu.2017.07.004
- Khuyagbaatar, B., Kim, K., Man Park, W., and Hyuk Kim, Y. (2016). Biomechanical Behaviors in Three Types of Spinal Cord Injury Mechanisms. *J. Biomech. Eng.* 138, 138. doi:10.1115/1.4033794
- Koser, D. E., Moendarbary, E., Hanne, J., Kuerten, S., and Franze, K. (2015). CNS Cell Distribution and Axon Orientation Determine Local Spinal Cord Mechanical Properties. *Biophysical J.* 108, 2137–2147. doi:10.1016/j.bpj.2015.03.039
- Kruse, S. A., Rose, G. H., Glaser, K. J., Manduca, A., Felmlee, J. P., Jack, C. R., et al. (2008). Magnetic Resonance Elastography of the Brain. *Neuroimage* 39, 231–237. doi:10.1016/j.neuroimage.2007.08.030
- Lam, C. J., Assinck, P., Liu, J., Tetzlaff, W., and Oxland, T. R. (2014). Impact Depth and the Interaction with Impact Speed Affect the Severity of Contusion Spinal Cord Injury in Rats. *J. Neurotrauma* 31, 1985–1997. doi:10.1089/neu.2014.3392
- Li, X.-F., and Dai, L.-Y. (2009). Three-Dimensional Finite Element Model of the Cervical Spinal Cord. *Spine* 34, 1140–1147. doi:10.1097/BRS.0b013e31819e2af1
- Li, X., Yang, B., Xiao, Z., Zhao, Y., Han, S., Yin, Y., et al. (2018). Comparison of Subacute and Chronic Scar Tissues after Complete Spinal Cord Transection. *Exp. Neurol.* 306, 132–137. doi:10.1016/j.expneurol.2018.05.008
- Lin, D. C., Shreiber, D. I., Dimitriadis, E. K., and Horkay, F. (2009). Spherical Indentation of Soft Matter beyond the Hertzian Regime: Numerical and Experimental Validation of Hyperelastic Models. *Biomech. Model. Mechanobiol.* 8, 345–358. doi:10.1007/s10237-008-0139-9
- Maikos, J. T., Elias, R. A. I., and Shreiber, D. I. (2008). Mechanical Properties of Dura Mater from the Rat Brain and Spinal Cord. *J. Neurotrauma* 25, 38–51. doi:10.1089/neu.2007.0348
- Maikos, J. T., Qian, Z., Metaxas, D., and Shreiber, D. I. (2008). Finite Element Analysis of Spinal Cord Injury in the Rat. *J. Neurotrauma* 25, 795–816. doi:10.1089/neu.2007.0423
- McKee, C. T., Last, J. A., Russell, P., and Murphy, C. J. (2011). Indentation versus Tensile Measurements of Young's Modulus for Soft Biological Tissues. *Tissue Eng. B: Rev.* 17, 155–164. doi:10.1089/ten.TEB.2010.0520
- Metz, H., McElhaney, J., and Ommaya, A. K. (1970). A Comparison of the Elasticity of Live, Dead, and Fixed Brain Tissue. *J. Biomech.* 3, 453–458. doi:10.1016/0021-9290(70)90017-5
- Noonan, V. K., Fingas, M., Farry, A., Baxter, D., Singh, A., Fehlings, M. G., et al. (2012). Incidence and Prevalence of Spinal Cord Injury in Canada: a National Perspective. *Neuroepidemiology* 38, 219–226. doi:10.1159/000336014
- Ozawa, H., Matsumoto, T., Ohashi, T., Sato, M., and Kokubun, S. (2001). Comparison of Spinal Cord Gray Matter and White Matter Softness: Measurement by Pipette Aspiration Method. *J. Neurosurg.* 95, 221–224. doi:10.3171/spi.2001.95.2.0221
- Persson, C., Summers, J., and Hall, R. M. (2011). The Importance of Fluid-Structure Interaction in Spinal Trauma Models. *J. Neurotrauma* 28 (1), 113–125. doi:10.1089/neu.2010.1332
- Prange, M. T., and Margulies, S. S. (2002). Regional, Directional, and Age-dependent Properties of the Brain Undergoing Large Deformation. *J. Biomech. Eng.* 124, 244–252. doi:10.1115/1.1449907
- Ramo, N. L., Shetye, S. S., Streijger, F., Lee, J. H. T., Troyer, K. L., Kwon, B. K., et al. (2018). Comparison of *In Vivo* and *Ex Vivo* Viscoelastic Behavior of the Spinal Cord. *Acta Biomater.* 68, 78–89. doi:10.1016/j.actbio.2017.12.024
- Ramo, N. L., Troyer, K. L., and Puttlitz, C. M. (2018). Viscoelasticity of Spinal Cord and Meningeal Tissues. *Acta Biomater.* 75, 253–262. doi:10.1016/j.actbio.2018.05.045
- Russell, C. M., Choo, A. M., Tetzlaff, W., Chung, T.-E., and Oxland, T. R. (2012). Maximum Principal Strain Correlates with Spinal Cord Tissue Damage in Contusion and Dislocation Injuries in the Rat Cervical Spine. *J. Neurotrauma* 29, 1574–1585. doi:10.1089/neu.2011.2225
- Saxena, T., Gilbert, J., Stelzner, D., and Hasenwinkel, J. (2012). Mechanical Characterization of the Injured Spinal Cord after Lateral Spinal Hemisection Injury in the Rat. *J. Neurotrauma* 29, 1747–1757. doi:10.1089/neu.2011.1818
- Scifert, J., Totoribe, K., Goel, V., and Huntzinger, J. (2002). Spinal Cord Mechanics during Flexion and Extension of the Cervical Spine: a Finite Element Study. *Pain Physician* 5, 394–400.
- Shetye, S. S., Troyer, K. L., Streijger, F., Lee, J. H. T., Kwon, B. K., Crompton, P. A., et al. (2014). Nonlinear Viscoelastic Characterization of the Porcine Spinal Cord. *Acta Biomater.* 10, 792–797. doi:10.1016/j.actbio.2013.10.038
- Shulyakov, A. V., Cenkowski, S. S., Buist, R. J., and Del Bigio, M. R. (2011). Age-dependence of Intracranial Viscoelastic Properties in Living Rats. *J. Mech. Behav. Biomed. Mater.* 4, 484–497. doi:10.1016/j.jmbbm.2010.12.012
- Simha, N. K., Jin, H., Hall, M. L., Chiravambath, S., and Lewis, J. L. (2007). Effect of Indenter Size on Elastic Modulus of Cartilage Measured by Indentation. *J. Biomech. Eng.* 129, 767–775. doi:10.1115/1.2768110
- Sjovold, S. G., Mattucci, S. F. E., Choo, A. M., Liu, J., Dvorak, M. F., Kwon, B. K., et al. (2013). Histological Effects of Residual Compression Sustained for 60 minutes at Different Depths in a Novel Rat Spinal Cord Injury

- Contusion Model. *J. Neurotrauma* 30, 1374–1384. doi:10.1089/neu.2013.2906
- van Dommelen, J. A. W., van der Sande, T. P. J., Hrapko, M., and Peters, G. W. M. (2010). Mechanical Properties of Brain Tissue by Indentation: Interregional Variation. *J. Mech. Behav. Biomed. Mater.* 3, 158–166. doi:10.1016/j.jmbbm.2009.09.001
- Yu, J., Manouchehri, N., Yamamoto, S., Kwon, B. K., and Oxland, T. R. (2020). Mechanical Properties of Spinal Cord Grey Matter and white Matter in Confined Compression. *J. Mech. Behav. Biomed. Mater.* 112, 104044. doi:10.1016/j.jmbbm.2020.104044

**Conflict of Interest:** The authors declare that the research was conducted in the absence of any commercial or financial relationships that could be construed as a potential conflict of interest.

**Publisher's Note:** All claims expressed in this article are solely those of the authors and do not necessarily represent those of their affiliated organizations, or those of the publisher, the editors and the reviewers. Any product that may be evaluated in this article, or claim that may be made by its manufacturer, is not guaranteed or endorsed by the publisher.

*Copyright © 2022 Jin, Zhu, Xu, Zheng, Zeng, Xie and Cheng. This is an open-access article distributed under the terms of the Creative Commons Attribution License (CC BY). The use, distribution or reproduction in other forums is permitted, provided the original author(s) and the copyright owner(s) are credited and that the original publication in this journal is cited, in accordance with accepted academic practice. No use, distribution or reproduction is permitted which does not comply with these terms.*